JACS
JOURNAL OF THE AMERICAN CHEMICAL SOCIETY

Communication

pubs.acs.org/JACS

Large-Scale Cubic InN Nanocrystals by a Combined Solution- and Vapor-Phase Method under Silica Confinement

Zhuo Chen,*[,†,§] Yanan Li,[†,§] Chuanbao Cao,*[,†] Songrui Zhao,[‡] Saeed Fathololoumi,[‡] Zetian Mi,[‡] and Xingyan Xu[†]

[†]Research Center of Materials Science, Beijing Institute of Technology, Beijing 100081, People's Republic of China

[‡]Department of Electrical and Computer Engineering, McGill University, 3480 University Street, Montreal, Quebec H3A 2A7, Canada

Supporting Information

ABSTRACT: Large-scale cubic InN nanocrystals were synthesized by a combined solution- and vapor-phase method under silica confinement. Nearly monodisperse cubic InN nanocrystals with uniform spherical shape were dispersed stably in various organic solvents after removal of the silica shells. The average size of InN nanocrystals is 5.7 ± 0.6 nm. Powder X-ray diffraction results indicate that the InN nanocrystals are of high crystallinity with a cubic phase. X-ray photoelectron spectroscopy and energy-dispersive spectroscopy confirm that the nanocrystals are composed of In and N elements. The InN nanocrystals exhibit infrared photoluminescence at room temperature, with a peak energy of ~0.62 eV, which is smaller than that of high-quality wurtzite InN (~0.65−0.7 eV) and is in agreement with theoretical calculations. The small emission peak energy of InN nanocrystals, as compared to other low-cost solution or vapor methods, reveals the superior crystalline quality of our samples, with low or negligible defect density. This work will significantly promote InN-based applications in IR optoelectronic device and biology.

Narrow band gap semiconductor nanocrystals are emerging as an important class of nanomaterials for fundamental research, optoelectronics, and biomedical applications.[1−3] Efficient multiple exciton generation induced by spatial confinement in narrow band gap semiconductor nanocrystals leads to substantial improvements in the performance of optoelectronic devices, such as solar cells and low-threshold lasers.[4,5] Increasing efforts are being devoted to synthesize narrow band gap II−VI, III−V, and IV−VI semiconductor nanocrystals, such as HgTe and $Cd_xHg_{1-x}Te$, InP and InAs, PbS, PbSe, and PbTe.[6−12] InN nanocrystals received considerable attention after the discovery of its narrow band gap of about 0.7 eV,[13,14] as opposed to the previously accepted ~1.9 eV.[15] Consequently, InN has possible applications in high-efficiency solar cells, light-emitting diodes, laser diodes, etc.[16−18] In addition, InN is considered as a promising candidate for biological and in vivo medical applications, due to its nontoxicity and its infrared emission in the optically transparent region of water and blood.[19]

Historically, polycrystalline InN was synthesized by radio frequency sputtering,[20] which results in high free electron concentration, significant oxygen contamination, and an absorption edge at about 1.9 eV.[21−24] Recently, high-quality crystalline InN has been grown by molecular beam epitaxy (MBE).[25,26] The typically observed band gap of high-quality wurtzite-InN grown by MBE is around 0.65−0.7 eV.[18,27] However, the quality of InN samples grown using low-cost solution or other vapor methods has still remained poor, characterized by significantly high energy emission peaks (~1.7−2.45 eV),[28−32] or even no luminescence, due to the presence of extremely large densities of dislocations, defects, and/or impurities.[33] Therefore, there still exists a huge challenge to synthesize high-quality InN nanocrystals using low-cost solution or vapor methods.

The low-cost synthesis of monodisperse InN nanocrystals with uniform size and shape is required to exploit its applications in optoelectronic devices and biology. So far, the synthesis of InN nanocrystals using solution-phase routes, including solvothermal,[28−30,33,34] hydrothermal,[31] and thermal decomposition of single[35,36] and two precursors,[32,37,38] has resulted in nonuniform size and morphology distribution of nanocrystals. For synthesis of InN nanocrystals with uniform distribution, it is important to have a very fast nucleation and relatively slow growth process, which requires the growth unit concentration to reach high supersaturation level. However, such a condition is very difficult to achieve for nitride nanocrystals, due to their strong covalent bonding and lack of suitable precursors. Although during the past few decades, various methods and precursors have been studied, the effective reaction with a control over group III elements and nitrogen in the solution has still remained difficult. The quality of nitride nanocrystals is, therefore, dramatically lower than that of II−VI semiconductor nanocrystals. Other feasible approaches for synthesis of nitride nanocrystals are vapor-phase methods,[39] including ammonolysis,[40] dc-arc plasma,[41] and reactive laser ablation.[42] Usually, ammonia is used for nitrogen source in the vapor-phase growth process. The relatively high growth temperature in vapor-phase methods helps overcome the reaction difficulty encountered by solution methods. However, unlike the solution-based methods (where the nucleation and growth process could be separated by choosing appropriate ligands and solvents), the vapor-phase methods usually result in

Received: September 27, 2011
Published: December 31, 2011

   dx.doi.org/10.1021/ja209072v | J. Am. Chem.Soc. 2012, 134, 780−783

nonuniform nanocrystal morphology due to poor control over the nucleation process. Moreover, the vapor-phase methods often encounter the aggregation problem due to the large surface energy of nanocrystals. It is concluded that each of the aforementioned methods for synthesis of monodisperse InN nanocrystals faces significant challenges in achieving well-defined size and shape. In this work, we have addressed these critical issues by exploiting a new synthesis approach that results in monodisperse InN nanocrystals with uniform size and morphology and superior optical quality.

The approach to grow InN nanocrystals proposed in this work combines solution- and vapor-phase methods under silica shell confinement (SVSC), as schematically shown in Figure 1a.

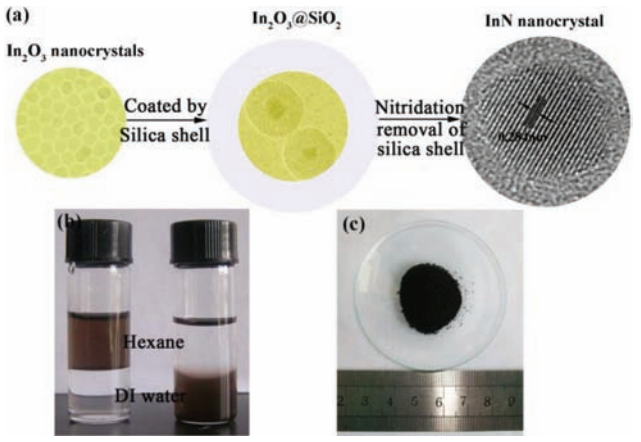

Figure 1. (a) Schematic of the SVSC method for InN nanocrystals. (b) The upper layer is hexane, and the bottom layer is distilled water. The left bottle contains InN nanocrystals in hexane, and the right one contains InN nanocrystals in water. (c) Large-scale InN@SiO_2 nanopowders (0.47 g) synthesized by the SVSC method.

In this method, the In_2O_3 nanocrystals with well-defined size and morphology were first synthesized by a solution-based method. In a typical reaction, indium-oleate (6 mmol), myristic acid (MA, 18 mmol), and 35 mL of 1-octadecene (ODE) were loaded in a 100 mL three-necked flask. The mixture was degassed and heated to 290 °C under a nitrogen atmosphere. When the temperature reached 290 °C, decyl alcohol (30 mmol) dissolved in 3 mL of ODE was quickly injected into the above mixture. The reaction was kept for 30 min and then stopped by removing the heater. Second, to overcome the nonuniform and aggregation problems associated with gas-phase growth, the In_2O_3 nanocrystals were coated by a silica shell before nitridation; this is because silica is inert and can be easily removed by HF acid. The obtained In_2O_3 nanocrystals were dispersed in 450 mL of hexane and then poured into a mixture of 45 mL of Triton X-100, 45 mL of hexanol, 3 mL of TEOS, and 13.5 mL of distilled water. After that, 1.5 mL of aqueous ammonia was added to catalyze the silica polymerization reaction. After the microemulsions were stirred at room temperature for 12 h, the nanocrystals were isolated by adding acetone. The specimens were dried under 80 °C, after removing the surfactant by centrifugation and washing using ethanol. The obtained In_2O_3@SiO_2 nanopowders were put into a tube furnace. After being purged with NH_3 gas for 20 min, the furnace was heated to 500−700 °C and kept for 5 h under NH_3 flow at 300 mL/min. Finally, large-scale InN@SiO_2 nanocrystals with uniform size and morphology were obtained through the SVSC route. After removal of the silica shell, InN nanocrystals can be dispersed into distilled water and then transferred to various nonpolar organic solvents by phase transfer, as shown in Figure 1b,c (around 0.47 g). To the best of our knowledge, this is the first report on the synthesis of large-scale and nearly monodisperse InN nanocrystals through the SVSC method. The SVSC method not only provides a unique tool for the synthesis of III nitride nanocrystals but also can be adopted for the growth of other functional nanocrystals with strong covalent bonding.

Figure 2a,b shows transmission electron microscopy (TEM) and high-resolution TEM (HRTEM) images of the InN

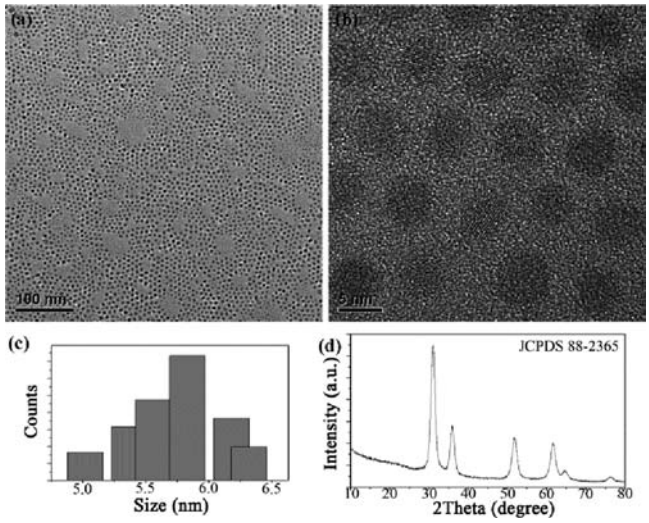

Figure 2. (a) Low-resolution TEM and (b) HRTEM images of the InN nanocrystals. (c) Size distribution of the InN nanocrystals. (d) XRD spectrum of the InN@SiO_2 nanocrystals obtained at 550 °C.

nanocrystals synthesized by the SVSC method at 550 °C, respectively. From the TEM images, the nanocrystals with nearly monodisperse spherical shape can be observed. Figure 2c shows the diameter distribution of the synthesized InN nanocrystals, revealing a fairly uniform size distribution of the nanocrystals from 5.0 to 6.3 nm. The average diameter of the nanocrystalls is calculated to be 5.7 ± 0.6 nm, after counting around 200 nanocrystals. Figures 1a and 2b reveal the highly crystalline nature of these InN nanocrystals. According to the lattice fringes of the InN nanocrystals, the lattice spacing between two planes is ∼0.28 nm, as shown in Figure 1a, corresponding to the distance of two {111} planes (JCPDS No. 88-2365).

Figure 2d shows the X-ray diffraction (XRD) pattern of the InN nanocrytals, which indicates the crystalline characteristics and phase of the InN@SiO_2 grown at 550 °C. All the peaks can be indexed to cubic InN (JCPDS No. 88-2365), except the broad peak at $2\theta = 22.5°$, which corresponds to the amorphous silica. No impurity peak of In_2O_3 was observed in the XRD pattern, meaning that all In_2O_3 nanocrystals had been converted to InN. We further investigated the effects of nitridation temperature on InN nanocrystals. Nitridation experiments were performed at 500, 550, 600, 650, and 700 °C. The color of synthesized InN nanocrystals gradually changes from red brown to dark as the nitridation temperature increases. The XRD results (see Supporting Information (SI) Figure S4) show that impurity peaks of In_2O_3 were observed for the sample with nitridation temperature of 500 °C, which means that In_2O_3@SiO_2 had not been converted completely to

dx.doi.org/10.1021/ja209072v | J. Am. Chem.Soc. 2012, 134, 780−783

InN@SiO_2. On the other hand, when the temperature was increased to 700 °C, the impurity peaks of indium appeared, indicating that indium was dissociated from the crystal. The indium metal from the high-temperature samples could even be seen by naked eyes. For nitridation temperatures of 550, 600, and 650 °C, no impurity peaks were found. For the In_2O_3 powders without silica shell, In_2O_3 was completely converted to InN at 500 °C. The nitridation temperature for In_2O_3 with silica shell is slightly higher than that of In_2O_3 without silica shell, which mainly stems from the fact that the silica shell hinders nitrogen atom diffusion. After normalizing the strongest peak (31°) at 550, 600, and 650 °C, respectively, the full widths at half-maxima (fwhm) of the peaks show similar values (see SI Figure S5), indicating that the temperature has a minor influence on the average particle size. Furthermore, the size of InN nanocrystals can also be controlled by the size of In_2O_3 nanocrystals. X-ray photoelectron spectroscopy (XPS) and energy-dispersive spectroscopy (EDS) confirmed that the nanocrystals were composed of elements In and N (see SI Figure S7 and S8).

Based on the above experimental results, encapsulation of In_2O_3 nanocrystals with the silica shells is indispensable for obtaining uniform shape and narrow size distribution of InN nanocrystals. If the In_2O_3 nanocrystals without silica shell were used as precursors, InN nanocrystals would aggregate and become coarse. Unlike the situation under silica shell confinement, the InN nanocrystals obtained by the In_2O_3 nanocrystals without silica shell exhibited hexagonal phase (see SI Figure S6), which suggests that the silica shell plays a key role in the formation of the cubic InN nanocrystals. Usually, the hexagonal phase is more stable than the cubic phase for group III nitrides. Therefore, nitridation of the In_2O_3 nanocrystals without silica shell preferentially forms hexagonal phase, as these atoms can be rearranged without any confinement. For nitridation of the In_2O_3@SiO_2 nanocrystals, there could exist an energy barrier to suppress atomic rearrangement due to the silica shell confinement. The energy barrier of phase change from cubic In_2O_3 to cubic InN could be lower than that of cubic In_2O_3 to hexagonal InN. Therefore, the formation of cubic InN nanocrystals should be attributed to the silica shell confinement, which suggests that the phase of InN nanocrystal can be controlled by adjusting the silica shell.

Photoluminescence (PL) properties of InN@SiO_2 nanocrystals in the form of powders (not in solutions) were investigated using micro-PL spectroscopy at room temperature. The sample was excited using a semiconductor laser ($\lambda \approx 635$ nm) through a 100× objective, and the PL emission was analyzed by a high-resolution spectrometer and an extended-range InGaAs detector with a lock-in amplifier. As illustrated in Figure 3, the InN@SiO_2 nanocrystals exhibit emission at room temperature. The fluctuation of PL signal at ~1900 nm could be due to water absorption and might not originate from the sample. The PL spectrum is characterized by the presence of three distinct emission peaks. The dominant emission peak is located at ~0.62 eV (~2.0 μm), which originates from the InN band edge emission. It has been known that the optical band gap of cubic InN is slightly smaller than that of wurtzite InN, which is in the range of ~0.65−0.7 eV.[18,27] Theoretically, the fundamental band gap of cubic InN is ~0.58 eV,[43] which is red-shifted to ~0.53 eV at 300 K, according to the Varshni's equation.[18] The observed ~90 meV blue-shift of the PL peak, i.e., the expected bulk value for cubic InN (~0.53 eV) at room temperature, to the present value (~0.62 eV) can be attributed

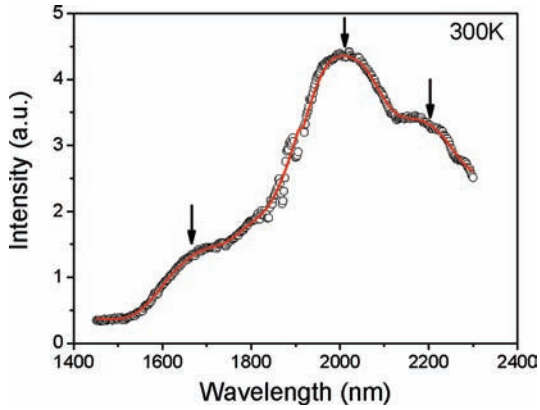

Figure 3. Photoluminescence spectrum of InN@SiO_2 nanocrystals at room temperature.

to quantum confinement effect. Additionally, the presence of defects and impurities may also lead to such a blue-shift, which has been commonly observed in n-type degenerate InN thin films and nanowires grown by MBE or metal−organic vapor-phase epitaxy.[44,45] The emission peak at ~0.75 eV (~1.65 μm) is likely related to the Mahan exciton emission[44] in the near-surface region of InN nanocrystals, where an electron accumulation layer may be present, as commonly observed on the surfaces of InN.[44−46] This results in a Fermi level that is positioned deep in the conduction band, thereby leading to a significant blue-shift in the PL spectrum, compared to the bandgap. Additionally, we have observed an emission peak at ~0.564 eV (~2.2 μm), which may be related to either an electron−phonon interaction[47] or an acceptor-band transition.[48] To our best knowledge, this is the first observation of strong IR emission (~0.62 eV) from InN nanocrystals prepared by any solution synthesis method. Other research groups, using similar solution- or vapor-phase methods, reported that the emission peaks were at ~1.84,[29] 1.9,[31] 1.7,[30] 2.2,[28] and 2.45 eV,[32] or even that there was no luminescence,[33] due to the presence of defects, dislocations, and/or oxygen contamination.

In summary, we have demonstrated the synthesis of large-scale InN nanocrystals with uniform spherical shape using a combined solution- and vapor-phase method under silica confinement. Nearly monodisperse InN nanocrystals were dispersed stably in various organic solvents after removal of the silica shells. The average size of InN nanocrystals is measured to be 5.7 ± 0.6 nm. The XRD results indicate that the In_2O_3@SiO_2 did not convert to InN@SiO_2 completely at 500 °C, and indium metal separated out at 700 °C. For 550, 600, and 650 °C, the InN nanocrystals exhibited high crystalline quality with cubic phase. Furthermore, XPS and EDS confirmed that the nanocrystals were composed of elements In and N. The InN@SiO_2 nanocrystals exhibited infrared PL at room temperature. The first successful synthesis of cubic InN nanocrystals with uniform morphology and size, together with IR emission at 0.62 eV, will greatly promote their applications in IR optoelectronic devices and biological imaging. Additionally, the SVSC method not only provides a road for synthesis of group III nitride nanocrystals, but also can be extended to prepare other functional nanocrystals with strong covalent bonding.

dx.doi.org/10.1021/ja209072v | J. Am. Chem.Soc. 2012, 134, 780−783

■ ASSOCIATED CONTENT

Supporting Information

Materials, experimental details, characterization data, and supporting figures. This material is available free of charge via the Internet at http://pubs.acs.org.

■ AUTHOR INFORMATION

Corresponding Author

zchen@bit.edu.cn.; cbcao@bit.edu.cn

Author Contributions

[§]These authors contributed equally to this work.

■ ACKNOWLEDGMENTS

This work was financially supported by the National Natural Science Foundation of China (Grant No. 51102017, 50972017 and 20471007), the Science Foundation for the Excellent Youth Scholars of Beijing Institute of Technology (Grant No. 2009Y0915), and 111 research base (BIT111-201101). Work performed at McGill was supported by the Natural Science and Engineering Research Council of Canada (NSERC). We thank Prof. Bingsuo Zou, Ruibin Liu, and Haizheng Zhong for optical measurements and helpful discussions.

■ REFERENCES

(1) Rogach, A.; Kershaw, S.; Burt, M.; Harrison, M.; Kornowski, A.; Eychmuller, A.; Weller, H. *Adv. Mater.* **1999**, *11*, 552−555.

(2) Sargent, E. H. *Adv. Mater.* **2005**, *17*, 515−522.

(3) Rogach, A. L.; Eychmuller, A.; Hickey, S. G.; Kershaw, S. V. *Small* **2007**, *3*, 536−557.

(4) Nozik, A. J. *Chem. Phys. Lett.* **2008**, *457*, 3−11.

(5) Nozik, A. J.; Beard, M. C.; Luther, J. M.; Law, M.; Ellingson, R. J.; Johnson, J. C. *Chem. Rev.* **2010**, *110*, 6873−6890.

(6) Battaglia, D.; Peng, X. *Nano Lett.* **2002**, *2*, 1027−1030.

(7) Xie, R.; Battaglia, D.; Peng, X. *J. Am. Chem. Soc.* **2007**, *129*, 15432−15433.

(8) Kim, S. W.; Zimmer, J. P.; Ohnishi, S; Tracy, J. B.; Frangioni, J. V.; Bawendi, M. G. *J. Am. Chem. Soc.* **2005**, *127*, 10526−10532.

(9) Allen, P. M.; Bawendi, M. G. *J. Am. Chem. Soc.* **2008**, *130*, 9240−9241.

(10) Xie, R.; Rutherford, M.; Peng, X. *J. Am. Chem. Soc.* **2009**, *131*, 5691−5697.

(11) Murphy, J. E.; Beard, M. C.; Norman, A. G.; Ahrenkiel, S. P.; Johnson, J. C.; Yu, P.; Mićić, O. I.; Ellingson, R. J.; Nozik, A. J. *J. Am. Chem. Soc.* **2006**, *128*, 3241−3247.

(12) Harris, D. K.; Allen, P. M.; Han, H.; Walker, B. J.; Lee, J.; Bawendi, M. G. *J. Am. Chem. Soc.* **2011**, *133*, 4676−4679.

(13) Matsuoka, T.; Okamoto, H.; Nakao, M.; Harima, H.; Kurimoto, E. *Appl. Phys. Lett.* **2002**, *81*, 1246−1248.

(14) Monemar, B.; Paskov, P. P.; Kasic, A. *Superlattice Microstruct.* **2005**, *38*, 38−56.

(15) Strite, S.; Morkoc, H. *J. Vac. Sci. Technol. B* **1992**, *10*, 1237−1266.

(16) Neff, H.; Semchinova, O. K.; Lima, A. M. N.; Filimonov, A.; Holzhueter, G. *Sol. Energy Mater. Sol. Cells* **2006**, *90*, 982−997.

(17) Nguyen, H. P. T; Chang, Y.-L; Shih, I.; Mi, Z. *IEEE J. Sel. Top. Quantum Electron.* **2011**, *17*, 1062.

(18) Wu, J. Q. *J. Appl. Phys.* **2009**, *106*, 011101.

(19) Michalet, X.; Pinaud, F. F.; Bentolila, L. A.; Tsay, J. M.; Doose, S.; Li, J.; Sundaresan, G.; Wu, A. M.; Gambhir, S. S.; Weiss, S. *Science* **2005**, *307*, 538−544.

(20) Hovel, H. J.; Cuomo, J. J. *Appl. Phys. Lett.* **1972**, *20*, 71.

(21) Tyagi, V. A.; Eustigneev, V. A.; Krasilo, A. M.; Andreeva, A. F.; Malatidiou, V. Y. *Sov. Phys. Semicond.* **1977**, *11*, 1257.

(22) Westra, K. L.; Lawson, R. P. W; Brett, M. J. *J. Vac. Sci. Technol. A* **1988**, *6*, 1730.

(23) Tansley, T. L.; Foley, C. P. *J. Appl. Phys.* **1986**, *59*, 3241.

(24) Morkoc, H. *Nitride Semiconductors and Devices*; Springer: Heidelberg, 1999.

(25) Chang, Y.-L.; Li, F.; Fatehi, A.; Mi, Z. *Nanotechnology* **2009**, *20*, 345203.

(26) Chang, Y.-L.; Mi, Z.; Li, F. *Adv. Funct. Mater.* **2010**, *20*, 4146.

(27) Cesar, M.; Ke, Y. Q.; Ji, W.; Guo, H.; Mi, Z. T. *Appl. Phys. Lett.* **2011**, *98*, 202107.

(28) Xiao, J.; Xie, Y.; Tang, R.; Luo, W. *Inorg. Chem.* **2003**, *42*, 107−111.

(29) Sardar, K.; Deepak, F. L.; Govindaraj, A.; Seikh, M. M.; Rao, C. N. R. *Small* **2005**, *1*, 91−94.

(30) Wu, C.; Li, T.; Lei, L.; Hu, S.; Liu, Y.; Xie, Y. *New J. Chem.* **2005**, *29*, 1610−1615.

(31) Xiong, Y.; Xie, Y.; Li, Z.; Li, X.; Zhang, R. *New J. Chem.* **2004**, *28*, 214−217.

(32) Greenberg, M. R.; Chen, W.; Pulford, B. N.; Smolyakov, G. A.; Jiang, Y.; Bunge, S. D.; Boyle, T. J.; Osinski, M. *Proc. SPIE* **2005**, *5705*, 68−76.

(33) Hsieh, J. C.; Yun, D. S.; Hu, E.; Belcher, A. M. *J. Mater. Chem.* **2010**, *20*, 1435−1437.

(34) Bai, Y.; Liu, Z.; Xu, X.; Cui, D.; Hao, X; Feng, X.; Wang, Q. *J. Cryst. Growth* **2002**, *241*, 189−192.

(35) Frank, A. C.; Stowasser, F.; Sussek, H.; Pritzkow, H.; Ambacher, C. R.; Giersig, M.; Fischer, R. A. *J. Am. Chem. Soc.* **1998**, *120*, 3512−3513.

(36) Sardar, K.; Dan, M.; Schwenzer, B.; Rao, C. N. R. *J. Mater. Chem.* **2005**, *15*, 2175−2177.

(37) Dingman, S. D.; Rath, N. P.; Markowitz, P. D.; Gibbons, P. C.; Buhro, W. E. *Angew. Chem., Int. Ed.* **2000**, *39*, 1470−1472.

(38) Chen, C.; Liang, C.; Tamkang, J. *Sci. Eng.* **2002**, *5*, 223−226.

(39) Bhaviripudi, S.; Qi, J.; Hu, E.; Belcher, A. M. *Nano Lett.* **2007**, *7*, 3512−3517.

(40) Schwenzer, B.; Meier, C.; Masala, O.; Seshadri, R.; DenBaars, S. P.; Mishra, U. K. *J. Mater. Chem.* **2005**, *15*, 1891−1895.

(41) Li, H.; Yang, H.; Yu, S.; Zou, G.; Li, Y.; Liu, S.; Yang, S. *Appl. Phys. Lett.* **1996**, *69*, 1285−1288.

(42) Goodwin, T. J.; Leppert, V. J.; Risbud, S. H.; Kennedy, I. M.; Lee, H. W. H. *Appl. Phys. Lett.* **1997**, *70*, 3122−3124.

(43) Bechstedt, F.; Furthmüller, J.; Ferhat, M.; Teles, L. K.; Scolfaro, L. M. R.; Leite, J. R.; Davydov, Y. V.; Ambacher, O.; Goldhahn, R. *Phys. Stat. Sol. (a)* **2003**, *195*, 628.

(44) Feneberg, M.; Däubler, J.; Thonke, K.; Sauer, R. *Phys. Rev. B* **2008**, *77*, 245207.

(45) Toma, S.; Ralph, J. M.; Raffaella, C.; Thomas, R.; Eli, S.; Hans, L. *Nano Lett.* **2006**, *6*, 1541.

(46)

(47) Holtz, M. E.; Gherasoiu, I.; Kuryatkov, V.; Nikishin, S. A.; Bernussi, A. A.; Holtz, M. W. *J. Appl. Phys.* **2009**, *105*, 036702.

(48) Wang, X. Q.; Che, S. B.; Ishitani, Y.; Yoshikawa, A. *Appl. Phys. Lett.* **2007**, *90*, 201913.